• Original Paper •

Impact of Long-range Desert Dust Transport on Hydrometeor Formation over Coastal East Asia

Zhenxi ZHANG[1,2], Wen ZHOU[3], Mark WENIG[4], and Liangui YANG[*1]

[1]*Research Institute of Fluid Dynamics, School of Mathematic Science, Inner Mongolia University, Hohhot 010021, China*

[2]*Department of Environmental Engineering, Inner Mongolia University of Technology, Hohhot 010010, China*

[3]*School of Energy and Environment, City University of Hong Kong, Hong Kong, Tat Chee Avenue, Kowloon, Hong Kong 999077, China*

[4]*Meteorologisches Institut, Ludwig-Maximilians-Universität, Munich 80539, Germany*

ABSTRACT

Model simulations and hydrological reanalysis data for 2007 are applied to investigate the impact of long-range desert dust transport on hydrometeor formation over coastal East Asia. Results are analyzed from Hong Kong and Shanghai, which are two representative coastal cities of East Asia. Long-range desert dust transport impacts mainly spring and summer clouds and precipitation over coastal East Asia. In spring, clouds and precipitation come mainly from large-scale condensation and are impacted mainly by dust from the Gobi, Sahara, and Thar deserts. These desert dusts can participate in the precipitation within and below the clouds. At lower latitudes, the dust particles act mainly as water nuclei. At higher latitudes, they act as both water nuclei and ice nuclei. The effect of Gobi, Sahara, and Thar dust on large-scale clouds and precipitation becomes stronger at higher latitudes. In summer, clouds and precipitation over coastal East Asia come mainly from convection and are impacted mainly by dust from the Taklamakan, Arabian, and Karakum-Kavir deserts. Most Taklamakan dust particles can participate in precipitation within convective clouds as ice nuclei, while Arabian and Karakum-Kavir dust particles participate only as water nuclei in precipitation below the clouds. The effect of Taklamakan dust on convective clouds and precipitation becomes stronger at lower latitudes. Of all the desert dusts, that from the Gobi and Taklamakan deserts has the relatively largest impact. Gobi dust impacts climate change in coastal East Asia by affecting spring water clouds at higher latitudes.

Key words: dust, transport, condensation nuclei, hydrometeor, East Asia

Citation: Zhang, Z. X., W. Zhou, M. Wenig, and L. G. Yang, 2017: Impact of long-range desert dust transport on hydrometeor formation over coastal East Asia. *Adv. Atmos. Sci.*, **34**(1), 101–115, doi: 10.1007/s00376-016-6157-0.

1. Introduction

Precipitation processes, in particular hydrometeor formation, depend strongly on the presence of aerosol particles, which provide the nuclei for most water droplets (called cloud condensation nuclei) and ice crystals (called ice nuclei) in the precipitation. If the condensed moisture in the atmosphere is not altered, an increase in aerosol particle concentration causes the production of small droplets, for example, a decrease in the cloud droplet effective radius by anthropogenic aerosols occurs globally (Takemura et al., 2005), and these small cloud droplet coalesce very inefficiently into raindrops. This direct microphysical effect results in the corresponding suppression of precipitation (Warner, 1968; Rosenfeld, 1999; Haywood and Boucher, 2000). Thermodynamically, the suppression of the coalescence of small droplets

also leads to a decrease in the freezing temperature of the supercooled water in the cloud and inhibits the formation of ice precipitation (Rosenfeld, 2000).

Desert dust, as one important kind of aerosol, has attracted a lot of research attention in terms of its effect on cloud (Huang et al., 2006a, 2006b, 2010b; Wang and Huang, 2009). Dust particles have the ability to suppress precipitation from warm clouds but accelerate precipitation from cold clouds (Rosenfeld et al., 2001), depending on the concentrations of dust particles that form water and ice nuclei. Laboratory studies have shown that desert dust can serve as efficient ice nuclei (Schaefer, 1949, 1954; Isono et al., 1959; Roberts and Hallett, 1968; Levi and Rosenfeld, 1996; Zuberi et al., 2002; Hung et al., 2003). As water nuclei, dust aerosols produce numerous small droplets and suppress rainfall (Rosenfeld et al., 2001). But when dust coalesces with other soluble aerosols, it can form large water nuclei, and the increase in this kind of dust will enhance precipitation (Levin et al., 1996; Rosenfeld et al., 2002). So, desert dust can enhance

---

* Corresponding author: Liangui YANG

  Email: yyb3006@sina.com

precipitation when it serves as ice nuclei and large water nuclei (Rosenfeld and Nirel, 1996).

Dust particles that remain in convective clouds can easily act as ice nuclei because they can reach the middle and upper troposphere (DeMott et al., 2003), where deep convective clouds occur at about $-36°C$ to $-38°C$ (Rosenfeld and Woodley, 2000). On the other hand, convective clouds are the most sensitive to the impact of dust on precipitation. There are two kinds of sinks for cloud water vapor: one is the conversion into precipitation, and the other is the loss due to mixing and evaporation with the ambient air. The intervention of dust, as nuclei, will break the balance between these two kinds of sinks and promote the conversion of water vapor into precipitation (Rosenfeld et al., 2001).

Because they are transported from major desert regions all around the globe, dust aerosols can influence precipitation in locations far removed from their source; in particular, coastal regions, where the precipitation process is often active (van den Heever et al., 2006). Here, we investigate the impact of the long-range transport of desert dust on hydrometeor formation over coastal East Asia. We apply the Global Ozone Chemistry Aerosol Radiation and Transport (GOCART) model to simulate the transport of dust particles originating from deserts in Asia and Africa, and we select two important cities to represent coastal East Asia: Hong Kong [centered at (22.25°N, 114.25°E) on the Pearl River Delta] and Shanghai [centered at (31.18°N, 121.48°E) on the Yangtze River Delta].

The objective of this study is to investigate which desert dust has the largest impact and to determine how it affects hydrometeor formation. To achieve this objective, we analyze mainly the impact of desert dust on the microphysics, formation mechanism, and climate change of the precipitation in Hong Kong and Shanghai, based on simulated results and observation data. For the microphysics, we compare the ability of each kind of desert dust to act as ice or water nuclei. For the formation mechanism, we compare the ability of each kind of desert dust to affect large-scale condensation precipitation or convective precipitation (see section 2). For climate change, we analyze the climatic effect of dust emission on clouds and precipitation. The satellite observation dataset and reanalysis hydrological dataset used in this study are introduced in section 2, while the description and validation of the GOCART model is given in sections 3 and 4, respectively. Analysis of the model results, reanalysis data, and observation data, including the characteristics of desert dust transport, desert dust effects on clouds and precipitation, and desert dust climatic effects, are presented in sections 5, 6, and 7, respectively, followed by conclusions in section 8.

2. Data

2.1. *Satellite observation datasets*

The satellite-observed aerosol data from MISR, the Ozone Monitoring Instrument (OMI), and CALIPSO are used in this study. MISR is a remote sensor designed to mon-

itor the long-term trends of atmospheric aerosol particle concentrations, including those formed by natural sources and by human activities (Diner et al., 1998; Martonchik et al., 1998). The total aerosol optical depth (AOD) at a wavelength of 555 nm from MISR Level 3 monthly $0.5° × 0.5°$ aerosol product data is used in this study. For the OMI UV Aerosol Index (UVAI) data, its positive value comes mainly from desert dust because the absorption by dust increases strongly toward the UV (Torres et al., 2007). CALIPSO collects high-resolution profiles of the optical properties of aerosols and clouds, and dust is distinguished from other types of aerosols by its high depolarization ratio (Winker et al., 2007; Yu et al., 2010, 2013). The CALIPSO Lidar Level 3 aerosol product data are used in this study and provide monthly mean profiles of aerosol optical properties in the troposphere below 12 km.

2.2. *Reanalysis hydrological dataset*

The Modern Era-Retrospective Analysis for Research and Applications (MERRA) dataset is a reanalysis for the satellite era using version 5 of GEOS DAS (data assimilation system), and it focuses on historical analyses of the hydrological cycle for a broad range of weather and climate time scales (Rienecker et al., 2011). The MERRA dataset used here is three-dimensional, with a resolution of 1.25° longitude by 1.25° latitude, and 42 vertical pressure levels.

MERRA data can distinguish two types of moist physical processes for clouds and precipitation: those produced by convection and those produced by large-scale condensation (Balkanski et al., 1993; Chin et al., 2000; Rienecker et al., 2008, 2011). The convective process is triggered by conditionally unstable conditions and results in an immediate updraft with compensatory subsidence. The large-scale condensation process is triggered by water vapor saturation in a fraction of the grid box, as diagnosed from the mean grid box humidity and an assumed subgrid distribution of temperature (Balkanski et al., 1993). In both processes, any water in excess of saturation is precipitated immediately. It should be noted that short-lived convective clouds are the most sensitive to the impact of aerosols on precipitation, because the rate of cloud water conversion into precipitation has to compete with the rate of cloud water loss due to mixing and evaporation with the ambient air. Large-scale synoptically forced cloud systems are typically longer lived, and thus less vulnerable to the detrimental impact of smoke and dust on the precipitation (Rosenfeld et al., 2001). There are two ways to form precipitation: one is direct moisture condensation, caused mainly by the convective updraft structure; the other is the conversion of clouds, involving both large-scale clouds and convective clouds (anvils).

3. Model description

The Georgia Tech/Goddard GOCART model is used to simulate the major aerosol components in the atmosphere (Allen et al., 1996; Chin et al., 2000; Ginoux et al., 2001;

Zhang et al., 2014). The continuity equation solved in the model includes the emission, chemistry, advection, convection, diffusion, dry deposition, and wet deposition of each aerosol component. The GOCART model is driven by the meteorological fields from the GEOS DAS. The GEOS DAS fields are actually global assimilated databases that are constrained by meteorological observations. Their extensive prognostic and diagnostic fields can be applied to chemistry transport models (Schubert et al., 1993). The horizontal resolution of the GOCART model in this study is 2° latitude by 2.5° longitude, and its vertical resolution is 30 layers.

There are six desert dusts considered in this study, and they are simulated depending on their respective emission regions as defined in Fig. 1. In this study, the desert dust particles in 2007 are simulated because the Gobi dust emission in 2007 can be considered representative of its climatological mean value (see section 7), while the impact of Gobi dust on hydrometeor formation over coastal East Asia is larger than other desert dusts (see section 6). For each desert dust, the model has a spin-up of 3 months (from October to December 2006) prior to the simulations (from January to December 2007) because it is initialized with near-zero mass.

3.1. *Dust emission*

The size distribution of dust particles in the model includes eight size bins: 0.1–0.18 μm, 0.18–0.3 μm, 0.3–0.6 μm, 0.6–1 μm, 1–1.8 μm, 1.8–3 μm, 3–6 μm, and 6–10 μm, with corresponding effective radii of 0.15, 0.25, 0.4, 0.8, 1.5, 2.5, 4, and 8 μm, respectively. The first four classes are combined into one group (0.1–1 μm), with an effective radius of 0.75 μm, in order to improve the numerical efficiency. The dust emission flux F_p of a size bin p is calculated by the empirical formulation mentioned by Gillette and Passi (1988):

$$F_p = S\, s_p u^2 (u - u_t) \quad \text{if } u > u_t ,\qquad (1)$$

where S denotes the probability source function, which is defined as the probability of the sediments being collected in concave topographic regions with a bald surface; s_p is the fraction of each size class p within the soil; and u is the horizontal wind speed at the surface. The parameter u_t is the threshold velocity to erode the soil, as determined by surface wetness and particle size:

$$u_t = 6.5 \sqrt{\frac{\rho_p - \rho_a}{\rho_a} g \Phi_p} (1.2 + 0.2 \lg \omega) \quad \text{if } \omega < 0.5 ,\qquad (2)$$

where ρ_a and ρ_p represent the air and particle densities, respectively; Φ_p denotes the particle diameter; and ω denotes the surface wetness. The distribution of dust emission from every desert in 2007 is exhibited in Fig. 1.

3.2. *AOD*

AOD, reflecting attenuation of sunlight by a column of aerosol, can serve as a measure of aerosol column concentration. Given the aerosol type, mass, and wavelength, the AOD τ can be calculated by the formulations listed below:

$$\tau = B M_d ;\qquad (3)$$
$$B = \frac{3QM}{4\rho r_e M_d} ;\qquad (4)$$

where r_e is defined as the particle effective radius; ρ is the particle density; Q is the extinction coefficient; M_d is the aerosol dry mass excluding the mass of water taken by the aerosol; M is the aerosol mass including the dry mass M_d and the mass of water uptaken by the aerosol; and B is called the specific or mass extinction coefficient ($m^2\ g^{-1}$), including all the humidification effects. Correspondingly, the value of B is related to the relative humidity (RH) and wavelength (Chin et al., 2002) and is calculated from the optical property database in the Global Aerosol Data Set under the Mie-scattering theory (Kopke et al., 1997).

3.3. *Wet deposition*

Wet deposition of aerosols in the model includes the removal processes of large-scale precipitation and convective precipitation. The calculation method for dust is the same as that used for sulfate (Ginoux et al., 2001). The aerosols scavenged by convective precipitation are computed according to the convective mass transport operator. When an air mass is pumped in wet convective updrafts, a fraction of its aerosols will deposit. This fraction is called the scavenging efficiency, the value of which is 50% in shallow wet convection (extending up to 2600 m altitude), and 100% in deep wet convection. The aerosols scavenged by large-scale precipitation are computed using a first-order loss operator, which is parameterized using the method of Giorgi and Chameides (1986).
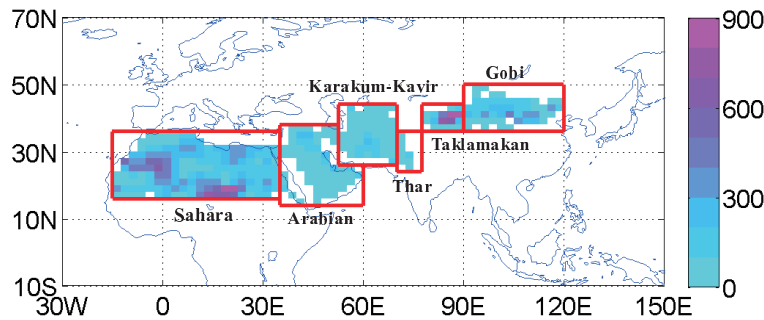

Fig. 1. Annual emissions (units: $g\ m^{-2}\ yr^{-1}$) of every desert in 2007 used in the GOCART model. The domains of each desert are shown in the red panels.

4. Comparison with satellite observations

To validate the GOCART model simulation for dust in 2007, it is compared with the satellite observation from MISR, OMI, and CALIPSO.

The total AOD at a wavelength of 555 nm from MISR is compared with the GOCART-simulated dust AOD at a wavelength of 550 nm (Fig. 2). To present the properties of dust distribution more accurately, OMI UVAI data are also involved in the comparison. The model can correctly reproduce the major dust plumes, in particular those emitted from the deserts in Africa and Asia, and can also correctly simulate the seasonal variation in the distribution of the dust plumes. On the other hand, the model overestimates by about 0.4 units for the Taklamakan dust AOD in spring, summer and autumn, and the Sahara dust AOD in autumn, while it underestimates by about 0.1–0.2 units for the Arabian dust AOD in summer.

The dust extinction from the GOCART simulation (550 nm) is compared with that from the CALIPSO Level 3 dataset (532 nm), and both are presented in a zonal vertical section at 40°N (Fig. 3). This section crosses the Gobi and Taklamakan deserts in China and the Karakum Desert in central Asia, and it is close to the Sahara and Arabian deserts in Africa and the Thar Desert in South Asia. The dust source in the model is located correctly at between 70°N and 110°N. The model can correctly reproduce the seasonal variation in the vertical and horizontal extension of the dust plume. In winter, the dust plume extends to only 2 km altitude, while it can extend to 4–5 km altitude in other seasons. The dust extinction in spring is larger than that in other seasons. Although the

model simulates the vertical and horizontal extensions of the dust plume observed by CALIPSO on a large scale at the correct place and time, it cannot capture the pronounced features on a small scale because their ranges are generally smaller than the model resolution. Consequently, the calculated dust extinction in the corresponding locations is smaller than the CALIPSO observation.

5. Characteristics of desert dust transport to coastal East Asia

The impact of desert dust on precipitation in Hong Kong and Shanghai obviously depends on the temporal and vertical distribution of dust in these two cities, which is closely related to the transport of dust particles from the various deserts to Hong Kong and Shanghai. Here, the horizontal and vertical distribution of desert dust on its transmission pathway is investigated to reveal the characteristics of dust transport, which will be helpful in understanding the temporal and vertical distribution of desert dust in Hong Kong and Shanghai.

5.1. Characteristics of desert dust horizontal transport

For each desert dust, by analyzing the seasonal variation of dust AOD distributions, we can find the season in which dust is transported eastward most evidently, as shown in Fig. 4. Dust from the Sahara, Arabian, and Karakum-Kavir deserts, emitted from North Africa and the Middle East, respectively, can transport eastward to coastal East Asia via the north and south sides of the Tibetan Plateau, while dust from
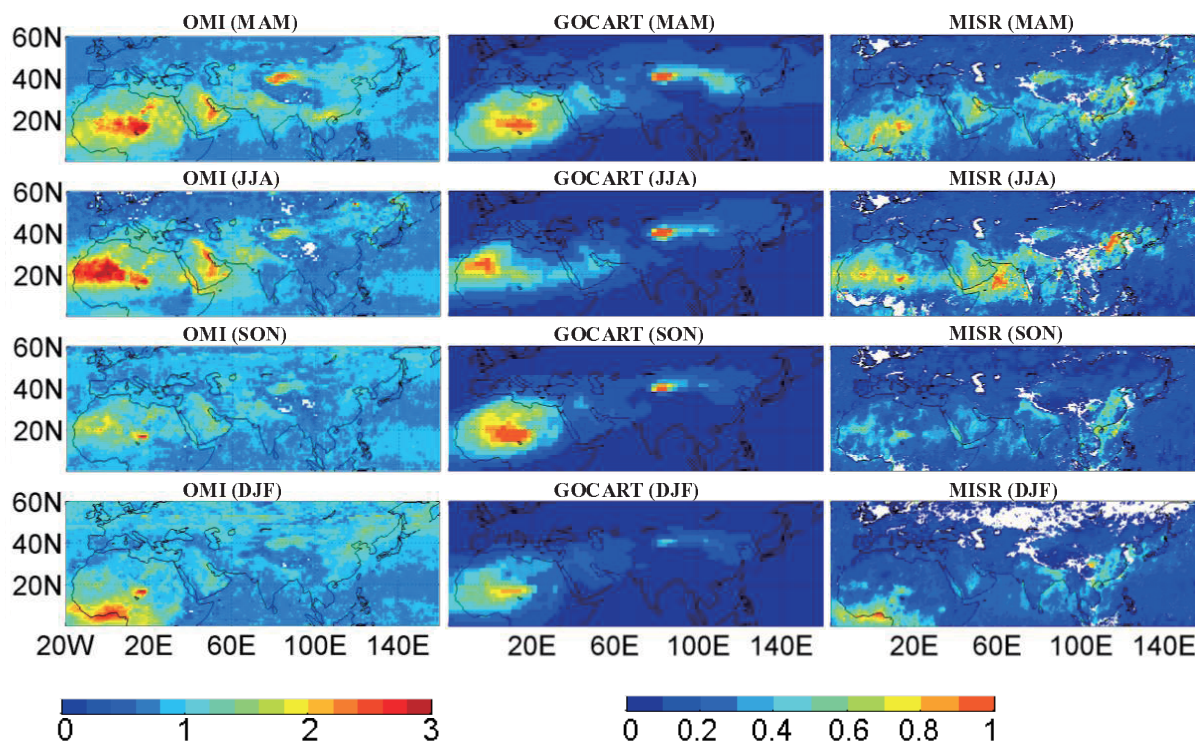

Fig. 2. Comparison between the seasonal distribution of the UV Aerosol Index from OMI observations, seasonal distribution of dust AOD (550 nm) from GOCART simulations, and seasonal distribution of AOD (555 nm) from MISR observations in 2007.
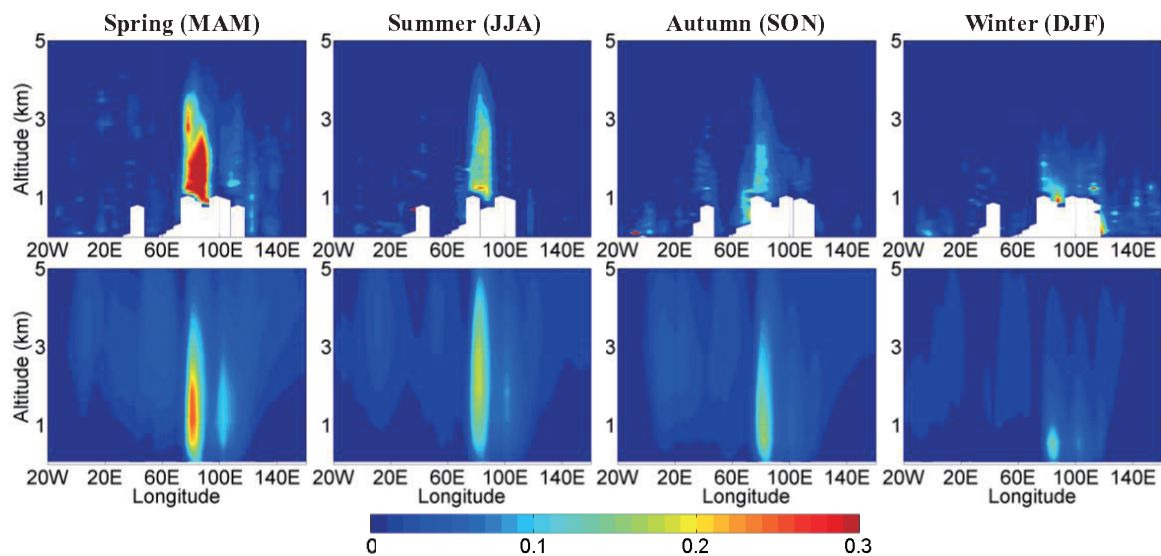
Fig. 3. Vertical section of dust extinction in 2007, at 40°N. The top row shows CALIPSO observations (532 nm), and the bottom row shows GOCART simulations (550 nm).

the Thar Desert, emitted from South Asia, can enter coastal East Asia only via the south side of the Tibetan Plateau. In China, Taklamakan and Gobi dust moves eastward and southward to coastal East Asia across the Mongolia Plateau.

Gobi dust moves to coastal East Asia in spring and winter, but the winter Gobi dust AOD over coastal East Asia is smaller than that in spring, because dust storms occurring in the Gobi desert in spring can make a large number of dust particles enter the atmosphere (Takemura et al., 2002; Lee et al., 2010). In spring, Gobi dust spreads correspondingly over much wider areas, into higher and lower latitudes, when it moves eastward. At lower latitudes, Gobi dust can reach East China and South China, and it enters Hong Kong and Shanghai obviously in May (see section 6).

Sahara dust can move to not only the Atlantic Ocean and North America (Perry et al., 1997; Prospero, 1999a, 1999b; Torres et al., 2002; Prospero and Lamb, 2003; Kaufman et al., 2005; Chin et al., 2007; Huang et al., 2010a), but also East Asia. The pathway of the Sahara dust transporting to East Asia includes a track from the eastern Mediterranean region to the Middle East subtropical jet, the polar jet, and the East Asian subtropical jet (Lee et al., 2011). The Sahara dust plume is divided into two branches when it passes across the Tibetan Plateau. The branch on the south side of the Tibetan Plateau stays in South Asia, while the branch on the north side moves continuously eastward across East Asia to the Pacific Ocean. This branch of the dust plume can enter coastal East Asia, especially East China and South China, in spring.

The extent of the area influenced by Taklamakan dust is small in winter and large in summer. In summer, Taklamakan dust spreads over a much wider latitudinal area and, at lower latitudes, it can reach coastal East Asia. In contrast to the Gobi dust transport controlled by the Asian monsoon, Taklamakan dust transport is controlled mainly by topography. West China is so high in altitude that the East Asian monsoon cannot affect it, so the movement of Taklamakan dust cannot be controlled by the monsoon.

Arabian and Karakum-Kavir dust can move to coastal East Asia not only via the south side of the Tibetan Plateau in summer, but also via the north side of the Tibetan Plateau in spring. But the eastward transport of Arabian dust is more evident in spring, because its emission in spring is stronger than those in other seasons, with the AOD value within the emission region being larger than that in other seasons, while the eastward transport of Karakum-Kavir dust is more evident in summer for the same reason. Thar dust is transported to coastal East Asia mainly in summer, also via the south side of the Tibetan Plateau.

5.2. *Characteristics of vertical dust distribution*

The vertical dust number concentration distribution is shown in three profiles. The zonal profile at 40°N can present the variability of dust number concentration when dust particles are transported eastward via the north side of the Tibetan Plateau. On the other hand, the zonal profile at 20°N shows the variability of dust number concentration when dust particles are transported eastward via the south side of the Tibetan Plateau (Fig. 4). The meridional profile at 115°E can show the variability of dust number concentration when desert dust is carried to East Asia (Fig. 5).

The AOD distribution has already revealed that the impact of Gobi dust on coastal East Asia occurs mainly in spring. The zonal vertical profile at 40°N further shows that a large number of dust particles can reach high levels. As indicated by the meridional vertical profile at 115°E, this dust plume gradually descends southward from the Mongolian Plateau (from 45°N to 47°N) to coastal South China (from 20°N to 25°N).

Sahara dust in spring shows evident eastward movement into East Asia and affects the coastal region. The zonal vertical profile at 40°N presents the vertical dust distribution after
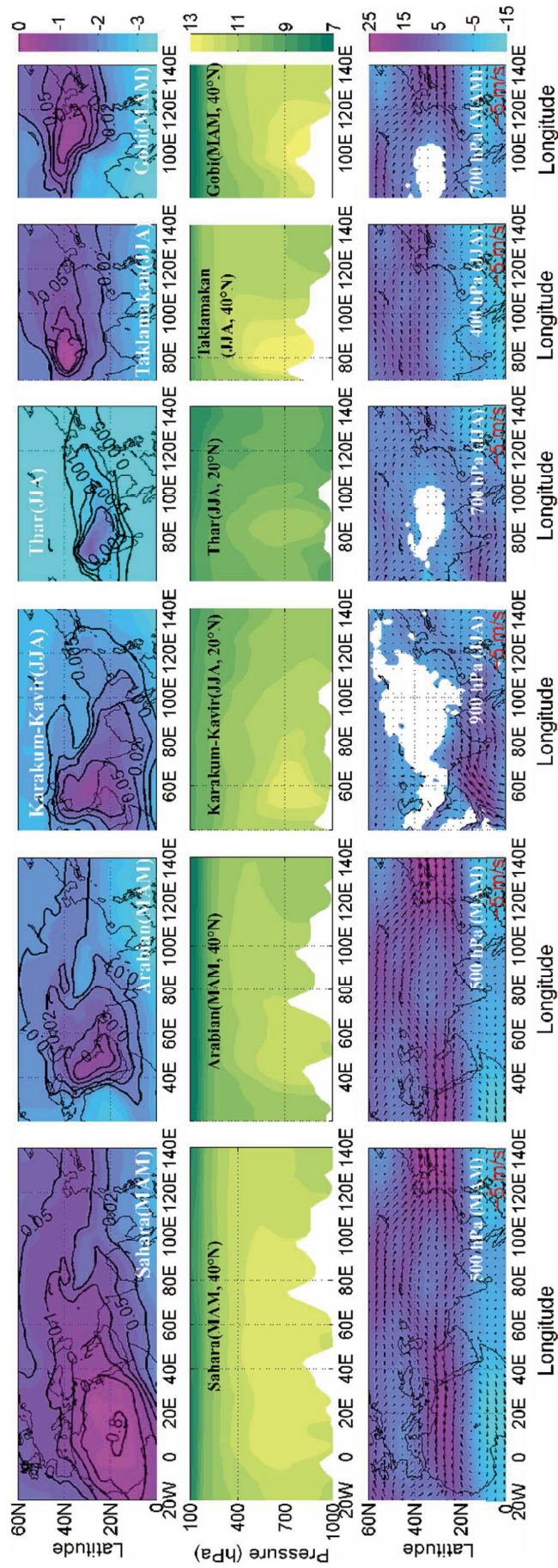
Fig. 4. Top: desert dust AOD (550 nm) distribution (on a logarithmic scale), in which the values of the solid lines are the AOD. Middle: dust number concentration (units: m^{-3}) distribution (on a logarithmic scale) in the zonal vertical profile at 20°N or 40°N. Bottom: wind vector field, in which the coloring shows the distribution of the eastward wind component (units: m s^{-1}).
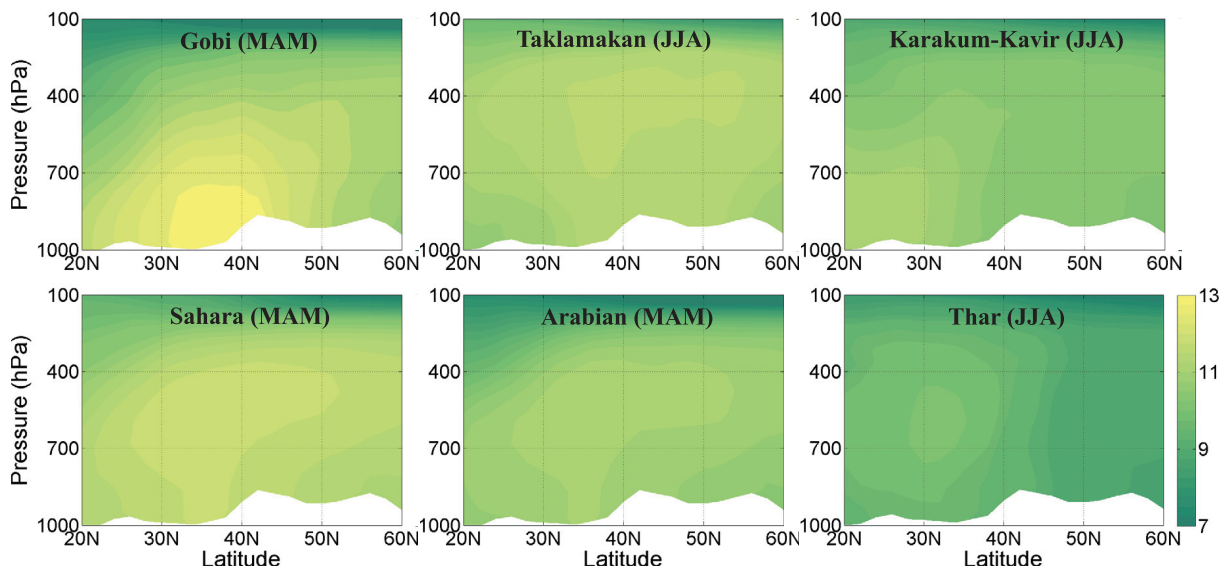
Fig. 5. Dust number concentration (units: m^{-3}) distributions (on a logarithmic scale) in the meridional vertical profile at 115°E.

it moves to East Asia via the north side of the Tibetan Plateau: when transported to East Asia, most Sahara dust particles are blocked by the plateau topography in China (from 60°E to 120°E), while only a few dust particles, which appear in the atmospheric layer above the plateaus, can continue to move eastward to coastal East Asia. The Sahara dust plume over the Mongolian Plateau, shown by the meridional vertical profile at 115°E, can range widely from ground level up to 300 hPa, and it can then gradually descend from upper levels to the ground when it spreads southward from the Mongolian Plateau to coastal South China.

The dust particles concentrate over the Taklamakan Basin (from 75°E to 95°E in the zonal vertical profile at 40°N), and in summer they can diffuse to high altitudes that far outstrip the Taklamakan Basin, and continue to move eastward to coastal East Asia. The meridional vertical profile at 115°E further shows that the dust plume over the Mongolian Plateau occurs mainly above 600 hPa and spreads to higher and lower latitudes.

Arabian dust enters East Asia in spring via the north side of the Tibetan Plateau. During this eastward movement, the Arabian dust plume appears mainly above 600 hPa (zonal vertical profile at 40°N in Fig. 4), and it occurs mainly over the Mongolian Plateau after entering China (Fig. 5).

Karakum-Kavir dust occurs in coastal East Asia mainly in summer, and its transport pathway is via the south side of the Tibetan Plateau. Correspondingly, the zonal vertical profile at 20°N shows the obvious eastward movement of Karakum-Kavir dust in summer, and the dust can even diffuse up to higher latitudes than other seasons, up to 400 hPa. Karakum-Kavir dust arrives in coastal South China only in the atmospheric layer close to the ground, but it can continuously spread northward into the atmospheric layer above 600 hPa (Fig. 5). Thar dust transports to coastal East Asia via the south side of the Tibetan Plateau in summer, which is similar to the Karakum-Kavir dust.

5.3. *Analysis of wind fields*

According to the dust number concentration distributions in the zonal vertical profile at 20°N or 40°N, we can find the altitudes where dust particles can be transported eastward over a long range of distance. For Sahara and Arabian dusts in spring, this altitude is at 500 hPa, while for Gobi dust it is at 700 hPa. For Karakum-Kavir, Thar, and Taklamakan dusts in summer, this altitude is at 900 hPa, 700 hPa, and 400 hPa, respectively. Therefore, the wind fields at these altitudes are shown in Fig. 4 and analyzed to understand the corresponding eastward transport of desert dust.

In spring, northwesterly wind prevails in the Gobi Desert, resulting in southeastward transport of Gobi dust to coastal East Asia. It is seen that the strong westerly wind passing through the Sahara and Arabian desert areas can carry the upper lofted dusts to move eastward, and these dusts are then carried eastward by the westerly wind at the north side of the Tibetan Plateau to reach coastal East Asia. In summer, as a consequence of the westerly wind prevailing at the northern side of the Indian Ocean, Karakum-Kavir and Thar dusts are transported eastward to pass through the south side of the Tibetan Plateau to reach East Asia. At the altitude of 400 hPa, the westerly wind north of 30°N can carry the upper lofted Taklamakan dust to move eastward, which is in agreement with the results of a modeling study on the transport of summer dust aerosols over the Tibetan Plateau (Liu et al., 2015).

6. Desert dust hydrometeor effects on coastal East Asia

6.1. *Effect of desert dust hydrometeors on Hong Kong*

In this section, the simulation results from the GOCART model, including the desert dust particle concentration and wet deposition over Hong Kong for 2007, are analyzed and connected with the monthly and vertical distribution of the
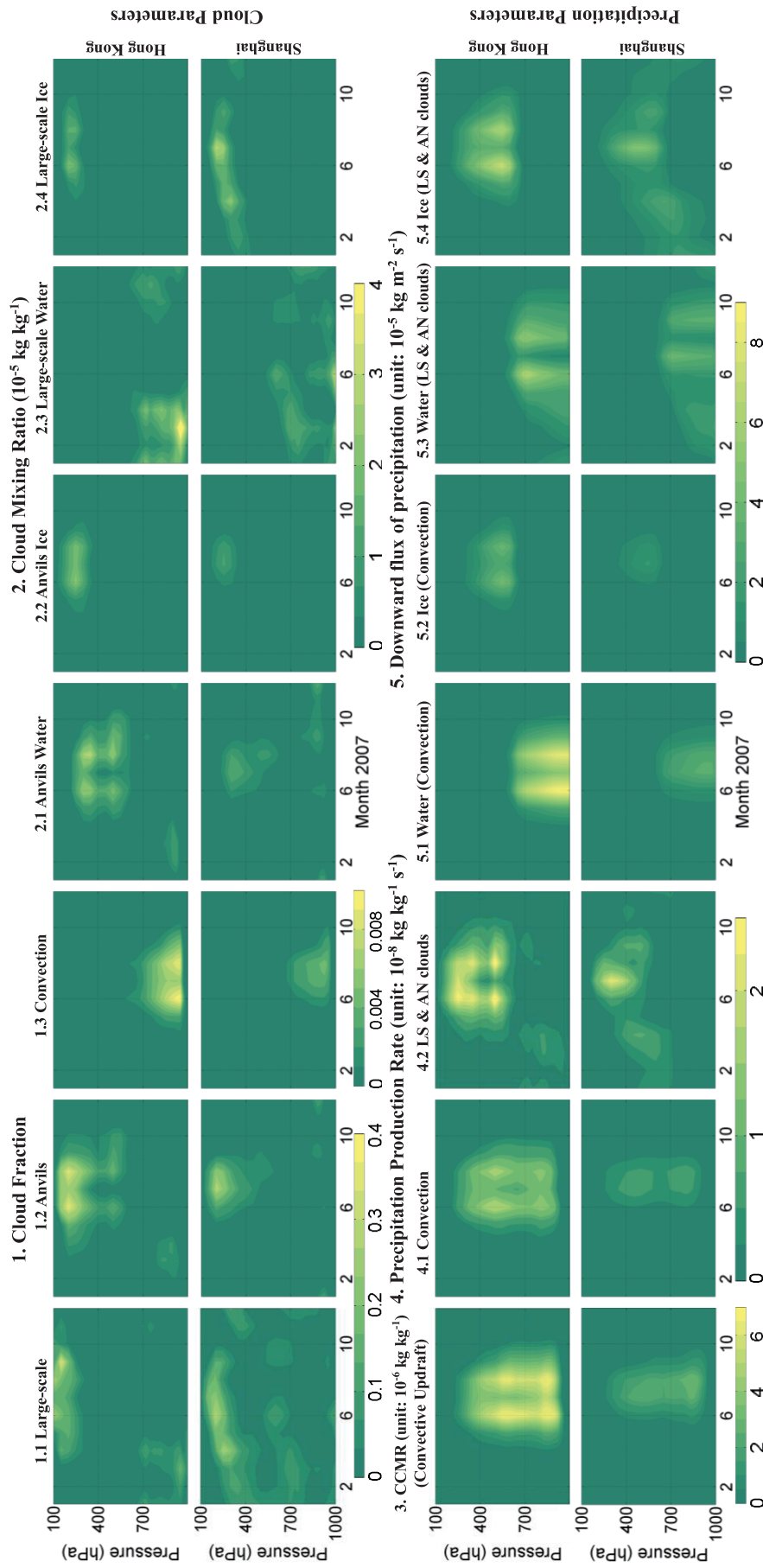
Fig. 6. Monthly variability of the vertical distribution of the clouds and precipitation parameters in 2007. "CCMR" means "Cloud Condensate Mixing Ratio", and "LS & AN" mean "Large-scale and anvils".

clouds and precipitation over Hong Kong in order to reveal the impact of desert dust on Hong Kong's clouds and precipitation.

6.1.1. *Properties of clouds and precipitation over Hong Kong in 2007*

The properties of clouds and precipitation over Hong Kong in 2007 are retrieved from the MERRA dataset. Fig. 6 first shows the temporal and vertical distribution of the fraction and mixing ratio of clouds. Hong Kong in spring is cloudier, with large-scale water clouds appearing mainly as fog below 600 hPa. The maximum of the cloud liquid water mixing ratio (4.78×10^{-5} kg kg^{-1}) occurs in March, at 950 hPa. Hong Kong in summer is humid except for July, when there is a fine dry spell. Therefore, June and August are the wettest months with a lot of clouds. Large-scale ice clouds are produced above 300 hPa. For anvil clouds, the classical and representative convective clouds, water and ice composition appear above 600 hPa and above 300 hPa, respectively.

Fig. 6 then shows the temporal and vertical distribution of the production rate and downward flux of precipitation. Rain in Hong Kong occurs mainly in summer, especially in June and August. Precipitation from anvils occurs above 600 hPa. On the other hand, precipitation from convective updraft structures is produced in the air column from 900 hPa to 300 hPa. In both convective and cloud conversion precipitation, the 600 hPa height is the boundary between ice and water precipitation.

Convective clouds and precipitation are very strong in summer because showers and thunderstorms often occur in Hong Kong during this time. On the other hand, Hong Kong is most likely to be affected by tropical cyclones, and when one of these storm centers nears Hong Kong, rain can become heavy and widespread and last for a few days.

6.1.2. *Impact of desert dust on Hong Kong's clouds and precipitation*

In connection with the distribution of clouds and precipitation over Hong Kong in 2007, we further discuss the impact of temporal, vertical, and particle radius variations of desert dust on Hong Kong precipitation, based on the vertical distribution of desert dust particle number concentration (Fig. 7) and dust wet deposition (Figs. 6 and 7) in Hong Kong in 2007.

6.1.2.1   Large-scale condensation

Gobi dust appears in Hong Kong mainly from April to May, and also from November to December, and it concentrates solely in the atmospheric layer below 700 hPa (Fig. 7). It is apparent that Gobi dust affects Hong Kong mainly in large-scale precipitation in spring. The wet deposition of Gobi dust comes mainly from large-scale precipitation and appears mainly in April, with particle radii generally smaller than 4 μm (Figs. 6 and 7). Because Gobi dust in spring exists in the same atmospheric layer as the clouds, where the temperature is higher than 0°C, Gobi dust affects the precipitation by acting as water nuclei rather than ice nuclei, and it

participates in the precipitation within the clouds.

6.1.2.2   Convection

The majority of Taklamakan dust arrives in Hong Kong in June, concentrating within the atmosphere layer between 600 hPa and 300 hPa (Fig. 7). Based on the position and timing of Taklamakan dust appearing in the atmosphere, it can be concluded that Taklamakan dust mainly impacts convective clouds and precipitation in Hong Kong. The majority of Taklamakan dust wet deposition in Hong Kong comes from convective precipitation, which is more than twice the value from large-scale precipitation (Fig. 8); and, it occurs mainly in June, with particle radii generally smaller than 4 μm (Fig. 9). In addition, the convective wet deposition of Taklamakan dust is greater than that of any other desert dust. Because of the condensation nuclei of precipitation and clouds, Taklamakan dust can act not only on the water liquid droplets, but also on the ice crystals, because it can arrive at high levels with temperatures of −30°C. Taklamakan dust is not passively washed by the rain below the clouds but participates actively in the formation of summer precipitation within the clouds.

Arabian and Karakum-Kavir dusts arrive in Hong Kong mainly in July and August, respectively. They correspondingly affect convective precipitation in Hong Kong. Both Arabian and Karakum-Kavir dusts occur below 600 hPa, under the cloud layer (Fig. 7), so they participate only in the precipitation below the clouds (washout). As far as microphysical characteristics, dust from both sources can act only as active liquid water nuclei because the atmospheric temperature where they occur is above 0°C.

6.1.2.3   Large-scale condensation and convection

Sahara dust arrives in Hong Kong mainly in May and December (Fig. 7), and May marks the transition period from spring precipitation to summer precipitation. Sahara dust correspondingly affects both large-scale precipitation and convective precipitation in Hong Kong. The wet deposition of Sahara dust from large-scale precipitation is obvious before May, while that from convective precipitation is apparent after May (Fig. 9). Also, the wet deposition of Sahara dust from large-scale precipitation is almost the same as that from convective precipitation (Fig. 8). Thar dust also occurs in May, so its impact on Hong Kong's precipitation is similar to that of Sahara dust, but with a smaller amount of wet deposition (Fig. 8).

6.2. *Effect of desert dust hydrometeors on Shanghai*

6.2.1. *Properties of clouds and precipitation over Shanghai in 2007*

Shanghai has a humid subtropical climate. In spring, the clouds in Shanghai are large-scale clouds, including water clouds appearing in March below 700 hPa and ice clouds appearing in April above 400 hPa (Fig. 6). In summer, Shanghai is hot and humid. Large-scale water clouds develop in June below 500 hPa, while large-scale ice clouds develop in July
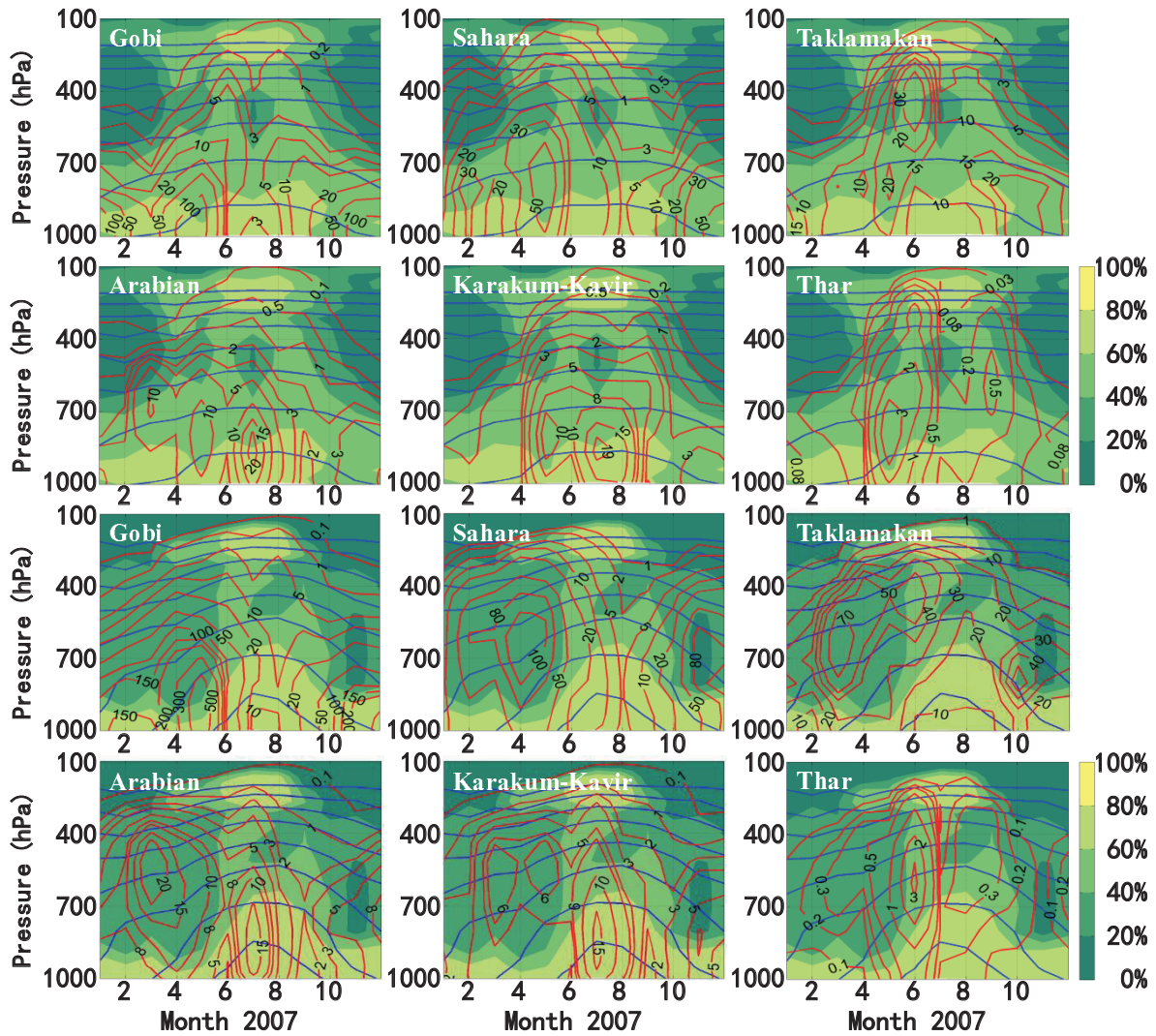
Fig. 7. Vertical and temporal distribution of number concentration (units: 10^{10} m^{-3}) of desert dust particles (red isolines) in Hong Kong (top two rows) and Shanghai (bottom two rows). The coloring presents the RH, while the blue lines are the isothermal lines at $-50°C$, $-40°C$, $-30°C$, $-20°C$, $-10°C$, $0°C$, $10°C$ and $20°C$, from high altitude to the surface.

above 300 hPa. In July, the water and ice composition of anvil clouds appears above 500 hPa and above 300 hPa, respectively. Autumn is generally sunny and dry, with a small number of large-scale water clouds developing in September below 500 hPa. Winter is chilly and damp, and large-scale water clouds exist in December below 700 hPa.

Shanghai is susceptible to large-scale precipitation in spring and autumn (Fig. 6). In spring, this precipitation is concentrated in March and April and its water composition occurs below 700 hPa. The large-scale precipitation in autumn is concentrated in September and its water composition occurs below 600 hPa. Convective precipitation occurs mainly in summer, when downpours, freak thunderstorms, and typhoons can be expected. Precipitation from anvils occurs in July above 500 hPa, and precipitation from convective updraft structures occurs in July and August and develops in the air column from 900 hPa to 300 hPa.

6.2.2. *Impacts of desert dust on Shanghai's clouds and precipitation*

6.2.2.1 Large-scale condensation

Gobi dust arrives in Shanghai mainly in spring and winter, with the particle concentration in May being greater than that in other months, and the dust plume can reach up to 400 hPa (Fig. 7). Gobi dust mainly affects large-scale clouds and precipitation over Shanghai, especially those in spring. The annual wet deposition of Gobi dust from large-scale precipitation is close to 1000 kg km^{-2}, while that from convective precipitation is only 200 kg km^{-2}. In addition, wet deposition of Gobi dust from large-scale precipitation occurs mainly in May, and the particle radii encompass all the dust bins of the GOCART model. The deposition from dust particles with a radius of 1.5 μm is larger than that from particles of other sizes (Figs. 6 and 7). Gobi dust affects the precipitation mi-

crophysically by acting as water and ice nuclei, and it participates in the precipitation both within and below the clouds.

Sahara dust arrives in Shanghai mainly in spring and winter, with the maximum dust particle concentration occurring in April, in the atmospheric layer from 800 hPa to 500 hPa (Fig. 7). Sahara dust correspondingly affects Shanghai's large-scale precipitation in spring. The wet deposition of Sahara dust from large-scale precipitation (285 kg km^{-2}) is obviously larger than that from convective precipitation (45 kg km^{-2}), and it occurs mainly in spring, especially in April, when the radius of deposited dust particles is generally smaller than 4 μm (Figs. 6 and 7). Sahara dust affects the precipitation microphysically by acting as water and ice nuclei, and it participates in the precipitation both within and below the clouds.

Thar dust arrives in Shanghai mainly in June and mainly affects large-scale clouds and precipitation. The corresponding wet deposition occurs mainly in spring, with particle radii generally smaller than 4 μm (Fig. 9). Because the dust exists above 700 hPa (Fig. 7), it can participate in the precipitation within the clouds, and it acts mainly as water nuclei.

6.2.2.2 Large-scale condensation and convection

Taklamakan dust arrives in Shanghai mainly in spring, summer, and autumn. The dust plume in June can reach very high levels, above 300 hPa (Fig. 7). Taklamakan dust in spring and autumn mainly impacts large-scale clouds and precipitation over Shanghai. The wet deposition of Taklamakan dust from large-scale precipitation occurs mainly from February to May, and also in October, with particle radii generally smaller than 4 μm (Fig. 9). When it reaches 500 hPa and exceeds the height of large-scale clouds, Taklamakan dust can participate actively in the formation of precipitation within the clouds. Because the majority of Taklamakan dust in spring occurs mainly in atmospheric layers with temperatures below 0°C, it affects the precipitation by acting as ice nuclei. On the other hand, Taklamakan dust in autumn affects the precipitation by acting as water nuclei, because the majority occurs mainly in atmospheric layers with temperatures above 0°C. Taklamakan dust in summer mainly impacts convective precipitation over Shanghai. The wet deposition of Taklamakan dust from convective precipitation occurs mainly in July and August, with particle radii gener-

ally smaller than 4 μm (Fig. 9). Because the dust plume can reach up to 400 hPa and can exceed the height of convective clouds, Taklamakan dust can affect the formation of precipitation within the clouds. Its microphysical effect on the precipitation mainly involves acting as ice nuclei. In contrast to the situation in Hong Kong, Taklamakan dust in Shanghai has a larger effect on large-scale precipitation than on convective precipitation: the annual wet deposition of Taklamakan dust from large-scale precipitation (223 kg km^{-2}) is larger than that of convective precipitation (98 kg km^{-2}) (Fig. 8).

Arabian dust arrives in Shanghai mainly in March and July, and that in March mainly affects large-scale precipitation. The wet deposition of Arabian dust from large-scale precipitation occurs mainly in March as well, and it is caused mainly by particles with a radius of 1.5 μm (Fig. 9). Arabian dust exists above 700 hPa, in the cloud layer (Fig. 7), so it can participate in the precipitation within and below the clouds. Microphysically, it acts mainly as ice nuclei because the atmospheric temperature where it occurs is below 0°C. Arabian dust in July mainly affects convective precipitation, and the wet deposition of Arabian dust from convective precipitation occurs mainly in July as well, with primary particle radii of 1.5 μm (Fig. 9). Arabian dust exists below 700 hPa (Fig. 7), so it participates only in the precipitation below the clouds. Microphysically, it acts mainly as water nuclei because the atmospheric temperature where it occurs is above 0°C.

6.2.2.3 Convection

Karakum-Kavir dust arrives in Shanghai mainly in July and mainly affects convective precipitation. Its corresponding wet deposition occurs mainly in July as well, with particle radii generally smaller than 2.5 μm (Fig. 9). Because the dust exists below 700 hPa (Fig. 7), it participates only in precipitation below the clouds. Microphysically, it acts mainly as water nuclei.

7. Climatic effect of desert dust on coastal East Asia

The formations of cloud and precipitation are important aspects of the hydrological cycle and climate; the long-term impact of dust on clouds or precipitation can reflect the ef-
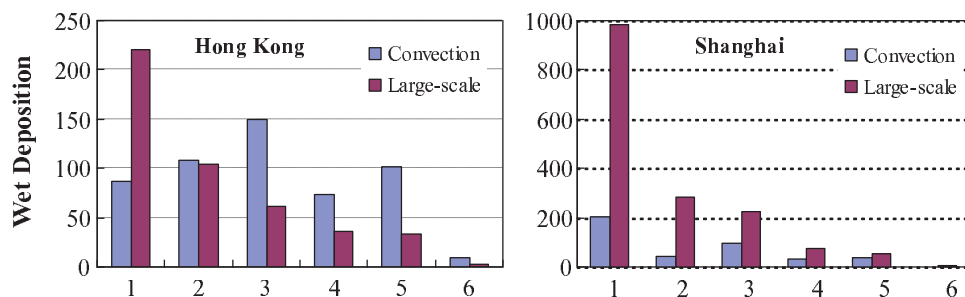

Fig. 8. Desert dust annual wet deposition (units: kg km^{-2}) over Hong Kong and Shanghai for 2007. The numbers on the x-axis represent the Gobi (1), Sahara (2), Taklamakan (3), Arabian (4), Karakum-Kavir (5), and Thar (6) deserts, respectively.
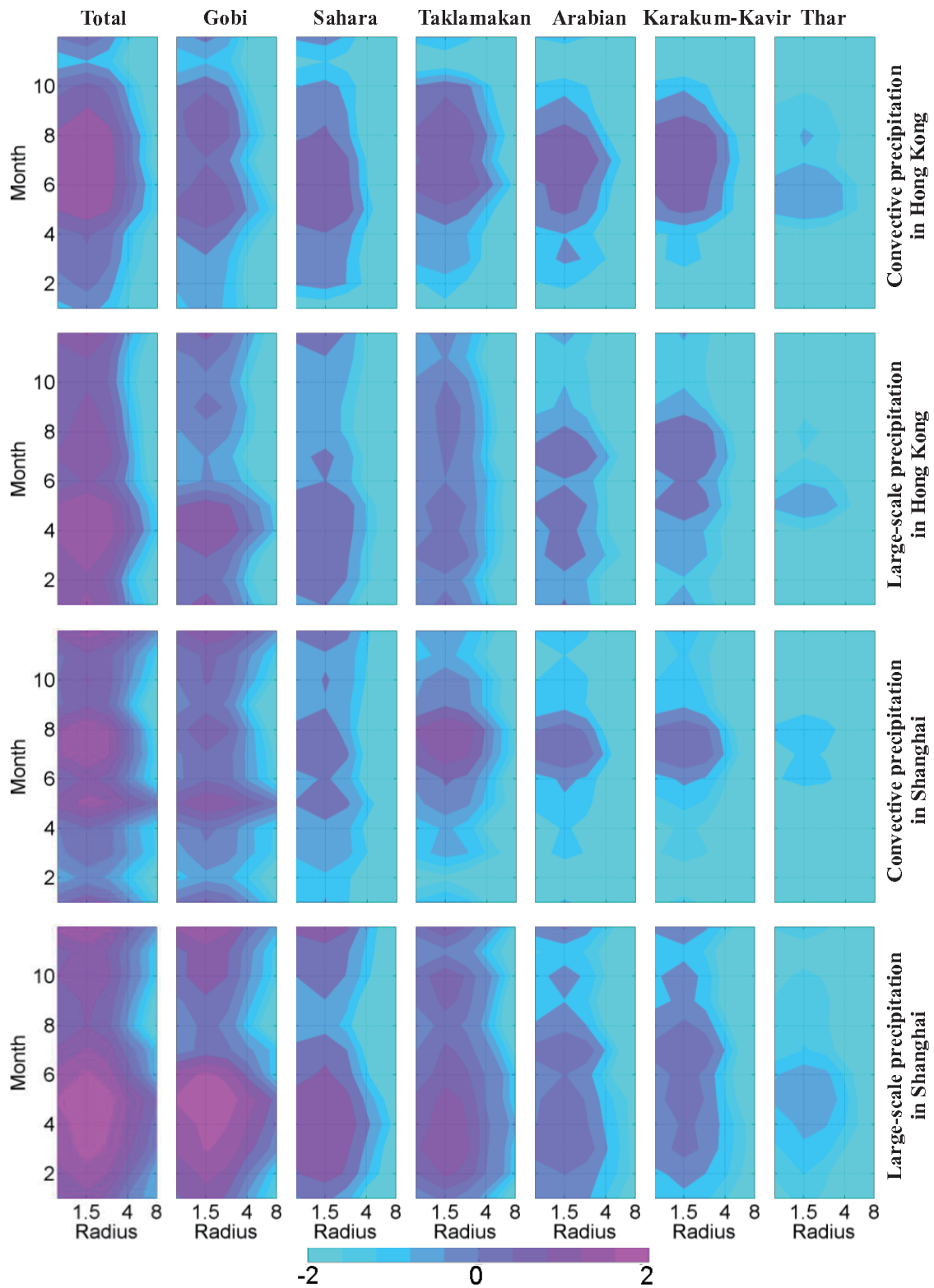
Fig. 9. Distribution (on a logarithmic scale) of dust wet deposition (units: kg km^{-2}) with time and dust particle radius.

fect of dust on the hydrological cycle and climate change of coastal East Asia.

Fig. 10 compares the interannual variability of the spring UVAI over the Gobi Desert and the integrated cloud water mixing ratio (from MERRA data) over Shanghai in April and May, from 1979 to 2013. The spring UVAI over the Gobi Desert (refer to Fig. 1) represents the dust emission and is calculated using the daily data from Total Ozone Meteorological Satellite (TOMS) (from 1979 to 2004) and OMI (from 2005 to 2013) satellite observations. The correlation
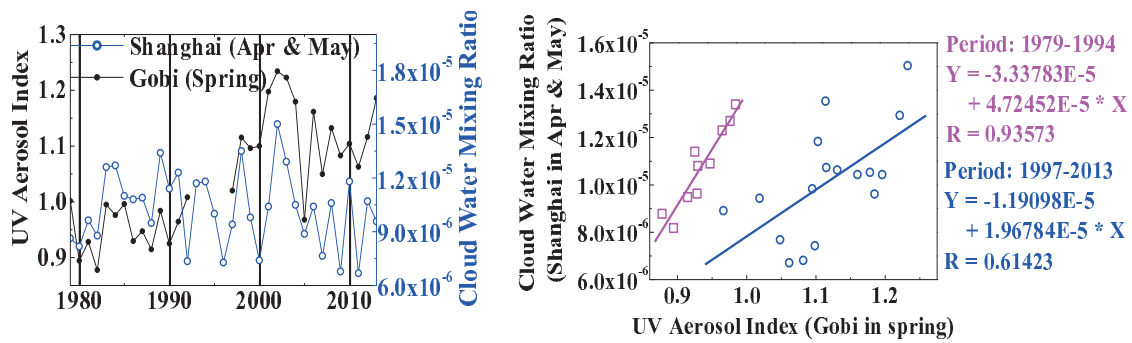
Fig. 10. Comparison between the interannual variability of the spring UV Aerosol Index over the Gobi desert and the integrated cloud water mixing ratio (units: kg kg^{-1}) over Shanghai in April and May from 1979 to 2013.

analysis shows that the integrated cloud water mixing ratio over Shanghai has a positive response to the spring Gobi dust emission, especially in the period from 1979 to 1994; the correlation coefficient is larger than 0.9 after screening out the extra UVAI data (>0.99). So, Gobi dust can impact climate change in Shanghai by affecting spring water clouds. The value of the OMI Aerosol Index over the Gobi desert region is 1.04953 in 2007, which is 95.8% of the temporal average value from 2005 to 2013 (1.095918). Therefore, the Gobi dust emission in 2007 can be considered as representative of its climatological mean value.

Of note is the response time of the cloud water mixing ratio over Shanghai to the spring Gobi dust emission, which includes the time taken for dust particles to transport from the emitting desert to Shanghai, and the time for dust particles to form the cloud condensation nuclei. Therefore, only the cloud water mixing ratio in April and May responds to spring Gobi dust emission, i.e., it excludes March, which is the response time. Another aspect is the effect of spatial position. In our study, the location is coastal East Asia, where the amount of cloud water probably has a positive response to the Asian dust load. However, over arid and semi-arid areas of East Asia, the situation is opposite: the amount of cloud water responds negatively to the Asian dust load because of the semi-direct effect of dust aerosol (Huang et al., 2006a).

8.   Summary and conclusions

The impact of long-range desert dust transport on the precipitation over coastal East Asia is investigated by analyzing simulation results and observation data over Hong Kong and Shanghai, which are representative coastal cities of East Asia. Six desert dusts are considered in this study: Gobi, Taklamakan, Sahara, Arabian, Karakum-Kavir, and Thar dust. Three aspects of their impact are discussed: precipitation microphysics, formation mechanism, and climate change. For microphysics, we compare every desert dust type's ability to act as an ice or water nucleus in precipitation. For the formation mechanism, we compare every desert dust's ability to affect large-scale precipitation or convective precipitation, as well as its ability to participate in precipitation formed within

or below clouds. Finally, we analyze the effect of desert dust on climate change in coastal East Asia via its impact on clouds or precipitation.

Long-range desert dust transport mainly impacts the spring and summer clouds and precipitation over coastal East Asia. In spring, clouds and precipitation over coastal East Asia come mainly from large-scale condensation and are impacted mainly by Gobi, Sahara, and Thar dust. At lower latitudes in coastal East Asia (Hong Kong), these desert dusts act mainly as water nuclei, because most of them appear in lower atmospheric layers with temperatures above 0°C. At higher latitudes (Shanghai), they can act as both water and ice nuclei, because the atmospheric temperature where they exist is lower, even below 0°C. Because spring clouds exist in lower atmospheric layers, these dusts correspondingly can participate in precipitation within and below the clouds. The effects of Gobi, Sahara, and Thar dust on large-scale clouds and precipitation become stronger at higher latitudes in coastal East Asia. In addition, at higher latitudes, Taklamakan and Arabian dusts appear in spring and mainly impact large-scale clouds and precipitation. They can participate in precipitation within the clouds, as ice nuclei.

In summer, clouds and precipitation over coastal East Asia come mainly from convection and are mainly impacted by Taklamakan, Arabian, and Karakum-Kavir dust. Most Taklamakan dust particles can participate in precipitation within convective clouds, as ice nuclei, because they arrive at high altitudes where the temperature is below 0°C. Arabian and Karakum-Kavir dusts occur mainly in the atmospheric layer below the cloud layer, with temperatures above 0°C; they participate only in precipitation below the clouds, and only as water nuclei.

Among all desert dusts, Gobi and Taklamakan dusts have the relatively largest impact on the clouds and precipitation over coastal East Asia. Furthermore, Gobi dust can even impact climate change in coastal East Asia by affecting spring water clouds at higher latitudes.

REFERENCES

Allen, D. J., P. Kasibhatla, A. M. Thompson, R. B. Rood, B. G. Doddridge, K. E. Pickering, R. D. Hudson, and S. J. Lin, 1996: Transport-induced interannual variability of carbon monoxide determined using a chemistry and transport model. *J. Geophys. Res.*, **101**, 28 655–28 669.

Balkanski, Y. J., D. J. Jacob, G. M. Gardner, W. C. Graustein, and K. K. Turekian, 1993: Transport and residence times of tropospheric aerosols inferred from a global three-dimensional simulation of ^{210}Ph. *J. Geophys. Res.*, **98**, 20 573–20 586.

Chin, M., R. B. Rood, S. J. Lin, J. F. Müller, and A. M. Thompson, 2000: Atmospheric sulfur cycle simulated in the global model GOCART: Model description and global properties. *J. Geophys. Res.*, **105**(D20), 24 671–24 687, doi: 10.1029/2000JD900384.

Chin, M., and Coauthors, 2002: Tropospheric aerosol optical thickness from the GOCART model and comparisons with satellite and sun photometer measurements. *J. Atmos. Sci.*, **59**, 461–483.

Chin, M., T. Diehl, P. Ginoux, and W. Malm, 2007: Intercontinental transport of pollution and dust aerosols: Implications for regional air quality. *Atmospheric Chemistry and Physics*, **7**, 5501–5517.

DeMott, P. J., K. Sassen, M. R. Poellot, D. Baumgardner, D. C. Rogers, S. D. Brooks, A. J. Prenni, S. M. Kreidenweis, 2003: African dust aerosols as atmospheric ice nuclei. *Geophys. Res. Lett.*, **30**(14), 1732, doi: 10.1029/2003GL017410.

Diner, D. J., and Coauthors, 1998: Multi-angle imaging Spectro-Radiometer (MISR) instrument description and experiment overview. *IEEE Trans. Geosci. Remote Sens.*, **36**, 1072–1087.

Gillette, D. A., and R. Passi, 1988: Modeling dust emission caused by wind erosion. *J. Geophys. Res.*, **93**, 14 233–14 242.

Ginoux, P., M. Chin, I. Tegen, J. M. Prospero, B. Holben, O. Dubovik, and S. J. Lin, 2001: Sources and distributions of dust aerosols simulated with the GOCART model. *J. Geophys. Res.*, **106**(D17), 20 255–20 273, doi: 10.1029/2000JD000053.

Giorgi, F., and W. L. Chameides, 1986: Rainout lifetimes of highly soluble aerosols and gases as inferred from simulations with a general circulation model. *J. Geophys. Res.*, **91**, 14 367–14 376.

Haywood, J., and O. Boucher, 2000: Estimates of the direct and indirect radiative forcing due to tropospheric aerosols: a review. *Rev. Geophys.*, **38**(4), 513–543.

Huang, J. P., B. Lin, P. Minnis, T. H. Wang, X. Wang, Y. X. Hu, Y. H. Yi, and J. R. Ayers, 2006a: Satellite-based assessment of possible dust aerosols semi-direct effect on cloud water path over East Asia. *Geophys. Res. Lett.*, **33**, doi: 10.1029/2006GL026561.

Huang, J. P., P. Minnis, B. Lin, T. H. Wang, Y. H. Yi, Y. X. Hu, S. Sun-Mack, and K. Ayers, 2006b: Possible influences of Asian dust aerosols on cloud properties and radiative forcing observed from MODIS and CERES. *Geophys. Res. Lett.*, **33**, L06824, doi: 10.1029/2005GL024724.

Huang, J. F., C. D. Zhang, and J. M. Prospero, 2010a: African dust outbreaks: A satellite perspective of temporal and spatial variability over the tropical Atlantic Ocean. *J. Geophys. Res.*, **115**, D05202, doi: 10.1029/2009JD012516.

Huang, J., P. Minnis, H. Yan, Y. Yi, B. Chen, L. Zhang, and J. K. Ayers, 2010b: Dust aerosol effect on semi-arid climate over Northwest China detected from A-Train satellite mea-surements. *Atmospheric Chemistry and Physics*, **10**, 6863–6872, doi: 10.5194/acp-10-6863-2010.

Hung, H.-M., A. Malinowski, and S. T. Martin, 2003: Kinetics of heterogeneous ice nucleation on the surfaces of mineral dust cores inserted into aqueous ammonium sulfate particles. *J. Phys. Chem. A*, **107**, 1296–1306.

Isono, K., M. Komabayasi, and A. Ono, 1959: The nature and origin of ice nuclei in the atmosphere. *J. Meteor. Soc. Japan*, **37**, 211–233.

Kaufman, Y. J., I. Koren, L. A. Remer, D. Tanré, P. Ginoux, and S. Fan, 2005: Dust transport and deposition observed from the Terra-Moderate Resolution Imaging Spectroradiometer (MODIS) spacecraft over the Atlantic Ocean. *J. Geophys. Res.*, **110**(D10), doi: 10.1029/2003JD004436.

Kopke, P., M. Hess, I. Schult, and E. P. Shettle, 1997: Global aerosol data set. MPI Meteorologie Hamburg Report No.243, 44 pp.

Lee, Y. C., X. Yang, and M. Wenig, 2010: Transport of dusts from East Asian and non-East Asian sources to Hong Kong during dust storm related events 1996-2007. *Atmos. Environ.*, **44**(30), 3728–3738.

Lee, Y. C., M. Wenig, Z. X. Zhang, N. Sugimoto, D. Larko, and T. Diehl, 2011: Dust episodes in Hong Kong (South China) and their relationship with the Sharav and Mongolian cyclones and jet streams. *Air Quality, Atmosphere & Health*, **5**(4), 413–424, doi: 10.1007/s11869-011-0134-7.

Levi, Y., and D. Rosenfeld, 1996: Ice nuclei, rainwater chemical composition, and static cloud seeding effects in Israel. *J. Appl. Meteor.*, **35**, 1494–1501.

Levin, Z., E. Ganor, and V. Gladstein, 1996: The effects of desert particles coated with sulfate on rain formation in the eastern Mediterranean. *J. Appl. Meteor.*, **35**, 1511–1523.

Liu, Y., Y. Sato, R. Jia, Y. Xie, J. Huang, and T. Nakajima, 2015: Modeling study on the transport of summer dust and anthropogenic aerosols over the Tibetan Plateau. *Atmospheric Chemistry and Physics*, **15**, 12 581–12 594.

Martonchik, J. V., D. J. Diner, R. A. Kahn, T. P. Ackerman, M. M. Verstraete, B. Pinty, and H. R. Gordon, 1998: Techniques for the retrieval of aerosol properties over land and ocean using multiangle imaging. *IEEE Trans. Geosci. Remote Sens.*, **36**, 1212–1227.

Perry, K. D., T. A. Cahill, R. A. Eldred, D. D. Dutcher, and T. E. Gill, 1997: Long-range transport of North African dust to the eastern United States. *J. Geophys. Res.*, **102**(D10), 11 225–11 238, doi: 10.1029/97JD00260.

Prospero, J. M., 1999a: Long-range transport of mineral dust in the global atmosphere: Impact of African dust on the environment of the southeastern United States. *Proceedings of the National Academy of Sciences of the United States of America*, **96**, 3396–3403, doi: 10.1073/pnas.96.7.3396.

Prospero, J. M., 1999b: Long-term measurements of the transport of African mineral dust to the southeastern United States: Implications for regional air quality. *J. Geophys. Res.*, **104**, 15 917–15 927, doi: 10.1029/1999JD900072.

Prospero, J. M., and J. P. Lamb, 2003: African droughts and dust transport to the Caribbean: Climate change implications. *Science*, **302**, 1024–1027, doi: 10.1126/science.1089915.

Rienecker, M. M., and Coauthors, 2008: The GEOS-5 data assimilation system — Documentation of versions 5.0.1, 5.1.0, and 5.2.0. Technical Rep. Series on Global Modeling and Data Assimilation. NASA Tech. Rep. 104606, Vol. 27, 101 pp.

Rienecker, M. M., and Coauthors, 2011: MERRA: NASA's

modern-era retrospective analysis for research and applications. *J. Climate*, **24**(14), 3624–3648, doi: 10.1175/JCLI-D-11-00015.1.

Roberts, P., and J. Hallett, 1968: A laboratory study of the ice nucleating properties of some mineral particulates. *Quart. J. Roy. Meteor. Soc.*, **94**, 25–34.

Rosenfeld, D., 1999: TRMM observed first direct evidence of smoke from forest fires inhibiting rainfall. *Geophys. Res. Lett.*, **26**(20), 3105–3108.

Rosenfeld, D., 2000: Suppression of rain and snow by urban and industrial air pollution. *Science*, **287**(5459), 1793–1796.

Rosenfeld, D., and R. Nirel, 1996: Seeding effectiveness—The interaction of desert dust and the southern margins of rain cloud systems in Israel. *J. Appl. Meteor.*, **35**, 1502–1510.

Rosenfeld, D., and W. L. Woodley, 2000: Deep convective clouds with sustained super-cooled liquid water down to $-37.5°C$. *Nature*, **405**(6785), 440–442.

Rosenfeld, D., Y. Rudich, and R. Lahav, 2001: Desert dust suppressing precipitation: a possible desertification feedback loop. *Proceedings of the National Academy of Sciences of the United States of America*, **98**(11), 5975–5980.

Rosenfeld, D., R. Lahav, A. Khain, and M. Pinsky, 2002: The role of sea spray in cleansing air pollution over ocean via cloud processes. *Science*, **297**, 1667–1670.

Schaefer, V. J., 1949: The formation of ice crystals in the laboratory and the atmosphere. *Chemical Reviews*, **44**, 291–320.

Schaefer, V. J., 1954: The concentrations of ice nuclei in air passing the summit of Mt. Washington. *Bull. Amer. Meteor. Soc.*, **35**, 310–314.

Schubert, S. D., R. B. Rood, and J. Pfaendtner, 1993: An assimilated dataset for earth science applications. *Bull. Amer. Meteor. Soc.*, **74**(12), 2331–2342.

Takemura, T., I. Uno, T. Nakajima, A. Higurashi, and I. Sano, 2002: Modeling study of long-range transport of Asian dust and anthropogenic aerosols from East Asia. *Geophys. Res. Lett.*, **29**, 11-1–11-4, doi: 10.1029/2002GL016251.

Takemura, T., T. Nozawa, S. Emori, T. Y. Nakajima, and T. Nakajima, 2005: Simulation of climate response to aerosol direct and indirect effects with aerosol transport-radiation model. *J. Geophys. Res.*, **110**, D02202, doi: 10.1029/2004JD005029.

Torres, O., P. K. Bhartia, J. R. Herman, A. Sinyuk, P. Ginoux, and B. Holben, 2002: A long-term record of aerosol optical depth from TOMS observations and comparison to AERONET measurements. *J. Atmos. Sci.*, **59**, 398–413.

Torres, O., A. Tanskanen, B. Veihelmann, C. Ahn, R. Braak, P. K. Bhartia, P. Veefkind, and P. Levelt, 2007: Aerosols and surface UV products from Ozone Monitoring Instrument observations: An overview. *J. Geophys. Res.*, **112**, D24S47, doi: 10.1029/2007JD008809.

van den Heever, S. C., G. G. Carrió, W. R. Cotton, P. J. DeMott, and A. J. Prenni, 2006: Impacts of nucleating aerosol on Florida storms. Part I: Mesoscale simulations. *J. Atmos. Sci.*, **63**(7), 1752–1775.

Wang, T. H., and J. P. Huang, 2009: A method for estimating optical properties of dusty cloud. *Chinese Optics Letters*, **7**(5), 368–372, doi: 10.3788/COL20090705.0368.

Warner, J., 1968: A reduction in rainfall associated with smoke from sugar-cane fires—An inadvertent weather modification?. *J. Appl. Meteor.*, **7**(2), 247–251.

Winker, D. M., W. H. Hunt, and M. J. McGill, 2007: Initial performance assessment of CALIOP. *Geophys. Res. Lett.*, **34**, L19803, doi: 10.1029/2007GL030135.

Yu, H. B., M. Chin, D. M. Winker, A. H. Omar, Z. Y. Liu, C. Kittaka, and T. Diehl, 2010: Global view of aerosol vertical distributions from CALIPSO lidar measurements and GOCART simulations: Regional and seasonal variations. *J. Geophys. Res.*, **115**, D00H30, doi: 10.1029/2009JD013364.

Yu, H. B., L. A. Remer, R. A. Kahn, M. Chin, and Y. Zhang, 2013: Satellite perspective of aerosol intercontinental transport: From qualitative tracking to quantitative characterization. *Atmospheric Research*, **124**, 73–100.

Zhang, Z. X., M. Wenig, W. Zhou, T. Diehl, K.-L. Chan, and L. N. Wang, 2014: The contribution of different aerosol sources to the Aerosol Optical Depth in Hong Kong. *Atmos. Environ.*, **83**, 145–154, doi: 10.1016/j.atmosenv.2013.10.047.

Zuberi, B., A. K. Bertram, C. A. Cassa, L. T. Molina, and M. J. Molina, 2002: Heterogeneous nucleation of ice in $(NH_4)_2SO_4$-H_2O particles with mineral dust immersions. *Geophys. Res. Lett.*, **29**, 142-1–142-4, doi: 10.1029/2001GL 014289.